Two-Stage Heat Pump using Oil-Free Turbocompressors – System Design and Simulation

Cordin ARPAGAUS[1]*, Stefan S. BERTSCH[1],
Adeel JAVED[2], Jürg SCHIFFMANN[2]

[1]NTB University of Applied Sciences of Technology Buchs
Institute for Energy Systems
Werdenbergstrasse 4, 9471 Buchs, Switzerland

[2] Ecole Polytechnique Fédérale de Lausanne
Laboratory for Applied Mechanical Design
Rue de la Maladière 71b, 2002 Neuchâtel, Switzerland

* Corresponding Author, E-mail: cordin.arpagaus@ntb.ch, Phone: +41 81 755 34 94

ABSTRACT

The combination of multi-stage heat pump cycles with small-scale oil-free turbocompressor technology running on gas bearings could be a promising way to increase performance in domestic and commercial heat pumps.
This paper presents a novel two-stage heat pump system with two heat sources at two different temperature levels using two separate turbocompressors rotating on gas bearings optimized for R134a. The system allows integration of unused heat sources, e.g. solar thermal or waste heat, into heat production with a minimal loss of exergy.
The cycle comprises an evaporator for the first heat source, a condenser as heat sink, an open economizer with integrated heat exchanger for the second heat source, and a tube-in-tube suction line heat exchanger (SHX) in the high-pressure for superheating and subcooling.
The aim of this study is to evaluate theoretically the performance of this heat pump cycle using a system model programmed in the software EES (Engineering Equations Solver). The simulation assumes steady-state, negligible pressure drops and heat losses, and adiabatic expansion processes. The superheating in the evaporator and the SHX is 5°C, and there is no subcooling in the condenser. The heat exchangers are modeled using effectiveness-NTU models.
At the design point, the heating capacity of the condenser is set to 6.5 kW and provides hot water of 55°C. The first heat source is brine of 5°C. The second heat source is water of 30°C and has been designed to provide up to 30% of the total condenser heat capacity.
The two turbocompressors are designed specifically to meet the heat pump design point. Presently, one-dimensional (1D) compressor maps are used in the heat pump model. Simulation results show that coefficient of performance (COP) improvements of 20% to 30% are achievable, depending on the source temperature levels of the heat pump cycle and the amount of second heat source added to the system.
The COP increases with higher source temperatures, higher second heat source capacity, and lower sink temperature. The pressure ratios are defined by the imposed temperature levels. The mass flow rate of the refrigerant in the first stage is mainly determined by the second heat source capacity, and in the second stage by the heat capacity of the condenser. In future work, this novel heat pump concept will be tested experimentally.

1. INTRODUCTION

1.1 Motivation

Heat pumps based on compression cycles are a key technology in domestic applications as they are highly energy efficient heat conversion devices. More and more, they are also spreading into the industrial sector, especially for waste heat recovery, heat upgrading, cooling and refrigeration in processes, or for heating applications of industrial buildings (IEA, 2012). Heat pumps with multi-temperature sinks and sources can cover various cooling and heating needs at the same time, as highlighted in a literature review by Arpagaus *et al.* (2016a, 2016b). Studies by several authors (Bertsch and Groll, 2008; Favrat *et al.*, 1997; Uhlmann *et al.*, 2014) showed that two-stage cycles outperform single stage cycles in terms of COP, especially when high temperature lifts are required. COP improvements of up to

30% were achieved by the addition of a second heat source (Uhlmann *et al.*, 2014). As stated by Bertsch and Groll (2008), a two-stage heat pump cycle with economizer provides a good compromise between cost, efficiency, and ease of installation. Major exergy losses in a heat pump cycle occur in the compressor (Schiffmann and Favrat, 2006). Oil-free direct driven small-scale turbomachinery has been identified as a technology that allows a significant performance increase in refrigeration and heat pump applications (Schiffmann, 2008). Major benefits beside the oil-free operation are the high compression efficiency and low exergy losses, as well as the hermetic, compact and lightweight design. Compressor technologies working with oil for lubrication lead to several disadvantages, such as oil degradation at high temperatures, reduction in compression efficiency, reduction in heat transfer performance, pressure losses in the heat exchangers, and oil migration issues in multi-stage cycles, thus making sophisticated oil management systems necessary (Zehnder, 2004).

Today, oil-free turbocompressors are an established technology in large scale heat pumps with 100 kW and higher heating capacity, e.g. in vapor recompression applications (Danfoss, 2013; GEA, 2014). Appropriate turbocompressors for domestic heat pumps in the small-scale range require the ability to operate on a wide range of inlet pressure, pressure ratios, and mass flows (Schiffmann and Favrat, 2010; Schiffmann, 2015). Studies by Schiffmann and Favrat (2010, 2009, 2006) demonstrated the technical feasibility of single-stage, small scale, oil-free and direct driven turbocompressors for integration in domestic heat pumps. Pressure ratios higher than 3.3 were reported with internal isentropic compressor efficiencies between 78% and 85%. The compressors run at high rotational speeds of up to 210'000 rpm in order to reach the necessary pressures. Recently, Carré (2015) integrated a twin-stage oil-free radial compressor unit in a domestic heat pump and demonstrated its technical feasibility for space heating application. Turbocompressors are therefore expected to be the next generation of compressors for small-scale heat pumps. Optimization potentials were recognized in the gas bearings and sealing design in order to achieve a long service life, high rotational speeds, and short maintenance times.

It follows that the combination of multi-stage heat pump cycles with small-scale oil-free turbocompressor technology running on gas bearings is a promising way to increase performance in domestic and commercial heat pumps (Schiffmann and Favrat, 2009; Schiffmann, 2014).

The aim of this paper is to go a step ahead and evaluate theoretically the performance of a two-stage heat pump system with two heat sources at two different temperature levels using two separate turbocompressors rotating on gas bearings optimized for R134a. The heat pump allows integration of unused heat sources, e.g. solar thermal or waste heat, into the heat production with a minimal loss of exergy.

1.2 System description

Figure 1 shows the schematic of the heat pump cycle along with the corresponding p-h diagram. The heat pump cycle follows a patent from Granwehr and Bertsch (2012), who propose heat pump systems that can incorporate several heat sources at different temperatures.

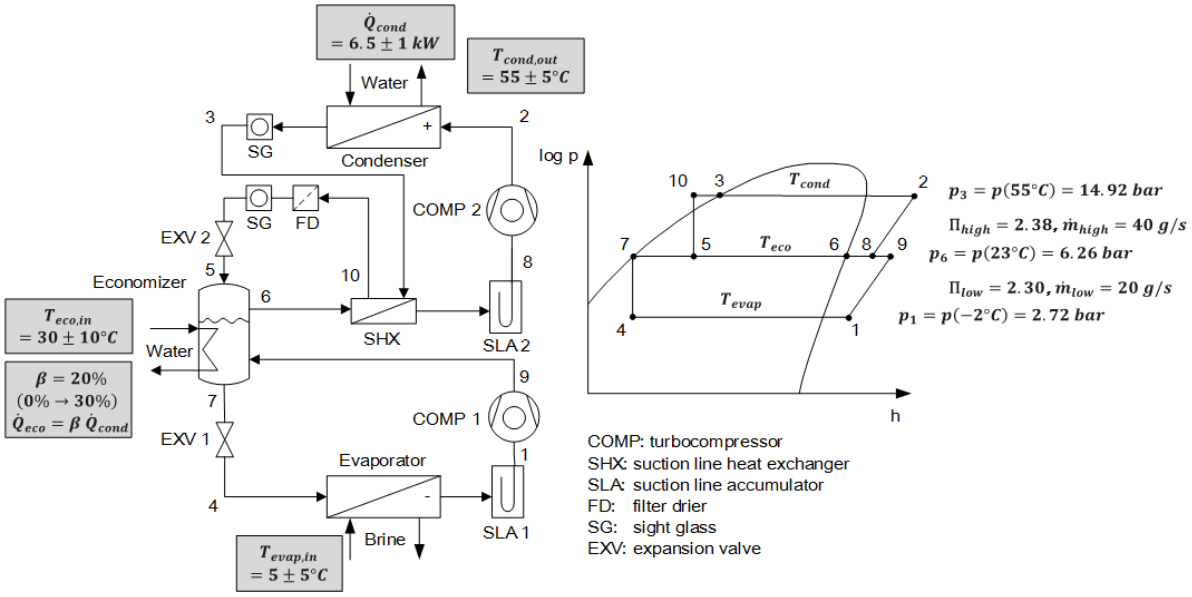

Figure 1: Schematic and p-h diagram of the two-stage heat pump cycle with turbocompressors at design conditions

The novelty of the heat pump cycle is the integration of two separate miniature turbocompressors in the first and second stage of the cycle. The oil-free turbocompressors are optimized for R134a. The cycle uses an evaporator for the first heat source, an open economizer with integrated heat exchanger for the second heat source, a suction line heat exchanger (SHX) in the second stage, and a condenser as heat sink. The refrigerant passes through suction line accumulators (SLA) before entering the compressors as a protection to prevent the injection of liquid droplets into the high-speed radial compressors (Schiffmann, 2008).
The discharge gas from the first stage compressor is directed into the open economizer to produce additional flash gas. The heat exchanger incorporated in the economizer allows heat transfer from the second heat source into the cycle at intermediate pressure. This heat evaporates additional refrigerant and increases the refrigerant flow towards the second stage. The tube-in-tube SHX ensures superheating of the vapor entering the second stage compressor, while at the same time, subcooling the liquid entering the expansion valve 2 (EXV 2).
After the condenser, a filter drier (FD) absorbs moisture and particles from the refrigerant. Sight glasses (SG) are used for liquid-phase control. The liquefied refrigerant released at the bottom of the economizer flows via the first stage expansion valve 1 (EXV 1) back to the evaporator for reheating, evaporation, and superheating and finally reenters the first stage compressor.

1.3 Design point conditions

As a case study, hot water is produced representing a potential waste heat recovery application for process or building heating. Table 1 lists the operating conditions of the heat pump at the design point.

Table 1: Operating conditions of the heat pump at the design point

Input parameter and variation range	Description
$\dot{Q}_{cond} = 6.5 \pm 1\ kW$	Heat sink capacity in the condenser
$T_{cond,out} = 55 \pm 5°$	Heat sink outlet temperature of the condenser (hot water)
$T_{eco,in} = 30 \pm 10°C$	2nd heat source inlet temperature of the economizer (water)
$T_{evap,in} = 5 \pm 5°C$	1st heat source inlet temperature of the evaporator (brine)
$\beta = 20\%\ (0\% \rightarrow 30\%)$	2nd heat source capacity factor in the economizer ($\dot{Q}_{eco} = \beta\ \dot{Q}_{cond}$)

Hot water of $T_{cond,out} = 55 \pm 5°C$ is produced by the heat pump using a fist heat source of $T_{evap,in} = 5 \pm 5°C$ (e.g. ground heat) and a second source heat of $T_{eco,in} = 30 \pm 10°C$ (e.g. waste heat from room heating or an industrial process). The heat sink capacity of the condenser is $\dot{Q}_{cond} = 6.5 \pm 1\ kW$, which fits the design point of the second stage turbocompressor for a mass flow rate of $\dot{m}_{high} = 40\ g/s$ (see Table 2). The process conditions would also correspond to a domestic heat pump application for hot water in low-energy houses, using for e.g. solar heat as the second source. The second source heat capacity $\dot{Q}_{eco}$ is defined with a capacity ratio $\beta = \dot{Q}_{eco}/\dot{Q}_{cond}$ of the heat capacity $\dot{Q}_{cond}$. Depending on the heat supply situation, β may vary between 0% and 30%. At the design point β is 20%.

Table 2: Design conditions of the turbocompressors (data from Javed *et al.* 2016)

Parameter	Symbol	Unit	1st stage compressor (*low*)	2nd stage compressor (*high*)
Mass flow rate R134a	$\dot{m}$	kg/s	0.02	0.04
Pressure ratio	Π	-	2.30	2.38
Inlet pressure	p	bar	2.72	6.26
Isentropic Efficiency	η	%	76.5	77.4
Design speed	n	rpm	227,000	235,000
Power	W_{el}	kW	0.49	0.96
Tip diameter of the impeller	D	mm	15.24	14.82

R134a is chosen as the refrigerant, as it allows acceptable compressor diameters of around 15 mm and moderate pressure ratios of about 2.3. R290 and R600a could also be considered for this application, as they are promising natural refrigerants and achieve higher temperature lifts. Compared to R290, the rotational speed with R134a is considerably lower, allowing higher electric efficiency in the electric motor drive (Schiffmann, 2008).

The turbocompressors used in this study have been designed specifically to meet the heat pump design requirements. Details about the design procedure of the turbocompressors is found in Javed *et al.* (2016). Presently, one-dimensional (1D) compressor map data are used in the heat pump model. Table 2 shows the design point data of the turbocompressors used in the two compressor stages.

2. EES MODEL

In order to evaluate this novel heat pump cycle, a system model has been developed and programmed in EES (Klein, 2012). The simulation model is based on the steady-state part models for each component of the cycle, as described in Bertsch and Groll (2006, 2008) and using the syntax of Klein and Nellis (2012).

2.1 Basic assumptions

The following assumptions were made:

- Pressure drops and heat losses are neglected ($p_1 = p_4$, $p_2 = p_3 = p_{10}$ and $p_5 = p_6 = p_7 = p_8 = p_9$).
- Refrigerant leaving the condenser is saturated liquid ($x_3 = 0$). Subcooling is established in the SHX.
- Superheating in the SHX and evaporator is 5°C.
- Economizer outlets are saturated vapor and liquid ($x_6 = 1, x_7 = 0$).
- Water and brine mass flows are in counter flow to the refrigerant.
- Brine is a 30% w/w ethylene glycol-water mixture (fluid properties calculated by brineprop2 in EES).
- Expansion devices are adiabatic leading to isenthalpic expansion processes ($h_5 = h_{10}, h_4 = h_7$).

2.2 Heat exchanger models

Overall effectiveness-NTU models are used to model the heat exchangers, which provides fast calculation and reasonably good results (Klein and Nellis, 2012). Table 3 shows the equations (1-20) used to determine the water (brine) mass flow rates, heat transfer coefficients, effectiveness, and NTU of the heat exchangers. The equations for the evaporator, economizer, and condenser are similar; for the SHX the ε-NTU relation for counter-flow conditions is applied. Energy balances on the components calculate the heat capacities (equations 1, 6, 11 and 16).
Figure 2 illustrates the selected temperature profiles in the heat exchangers at the design point conditions with the corresponding approach temperatures and temperature differences across the heat exchangers. Table 4 summarizes the determined values at the design conditions. The heat transfer coefficient values and mass flow rates of the supply and sink were kept constant in the calculations.

Table 3: Effectiveness-NTU equations for the heat exchangers used in the simulation model

Condenser		**Evaporator**	
$\dot{Q}_{cond} = \dot{m}_{high}(h_2 - h_3)$	(1)	$\dot{Q}_{evap} = \dot{m}_{low}(h_1 - h_4)$	(11)
$\varepsilon_{cond} = 1 - e^{-NTU_{cond}}$	(2)	$\varepsilon_{evap} = 1 - e^{-NTU_{evap}}$	(12)
$NTU_{cond} = UA_{cond}/\dot{m}_{cond}\, c_{P,cond}$	(3)	$NTU_{evap} = UA_{evap}/\dot{m}_{evap} c_{P,evap}$	(13)
$\dot{Q}_{cond} = \varepsilon_{cond}\, \dot{m}_{cond}\, c_{P,cond}\,(T_{cond} - T_{cond,in})$	(4)	$\dot{Q}_{evap} = \varepsilon_{evap}\, \dot{m}_{evap} c_{P,evap}\,(T_{evap,in} - T_{evap})$	(14)
$\dot{Q}_{cond} = \dot{m}_{cond}\, c_{P,cond}\,(T_{cond,out} - T_{cond,in})$	(5)	$\dot{Q}_{evap} = \dot{m}_{evap} c_{P,evap}\,(T_{evap,in} - T_{evap,out})$	(15)
Economizer		**SHX**	
$\dot{Q}_{eco} + \dot{m}_{low}(h_9 - h_7) + \dot{m}_{high}(h_5 - h_6) = 0$	(6)	$\dot{Q}_{SHX} = \dot{m}_{high}(h_8 - h_6) = \dot{m}_{high}(h_3 - h_{10})$	(16)
$\varepsilon_{eco} = 1 - e^{-NTU_{eco}}$	(7)	$\varepsilon_{SHX} = \frac{1 - e^{-NTU_{SHX}(1 - C_{SHX,r})}}{1 - C_{SHX,r}\, e^{-NTU_{SHX}(1 - C_{SHX,r})}}$	(17)
$NTU_{eco} = UA_{eco}/\dot{m}_{eco}\, c_{P,eco}$	(8)	$C_{SHX,r} = \dot{m}_{high}\, c_{P,6}/\dot{m}_{high}\, c_{P,3} < 1$	(18)
$\dot{Q}_{eco} = \varepsilon_{eco}\, \dot{m}_{eco}\, c_{P,eco}\,(T_{eco,in} - T_{eco})$	(9)	$NTU_{SHX} = UA_{SHX}/\dot{m}_{high}\, c_{P,6}$	(19)
$\dot{Q}_{eco} = \dot{m}_{eco} c_{P,eco}\,(T_{eco,in} - T_{eco,out})$	(10)	$\dot{Q}_{SHX} = \varepsilon_{SHX}\, \dot{m}_{high}\, c_{P,6}\,(T_3 - T_6)$	(20)

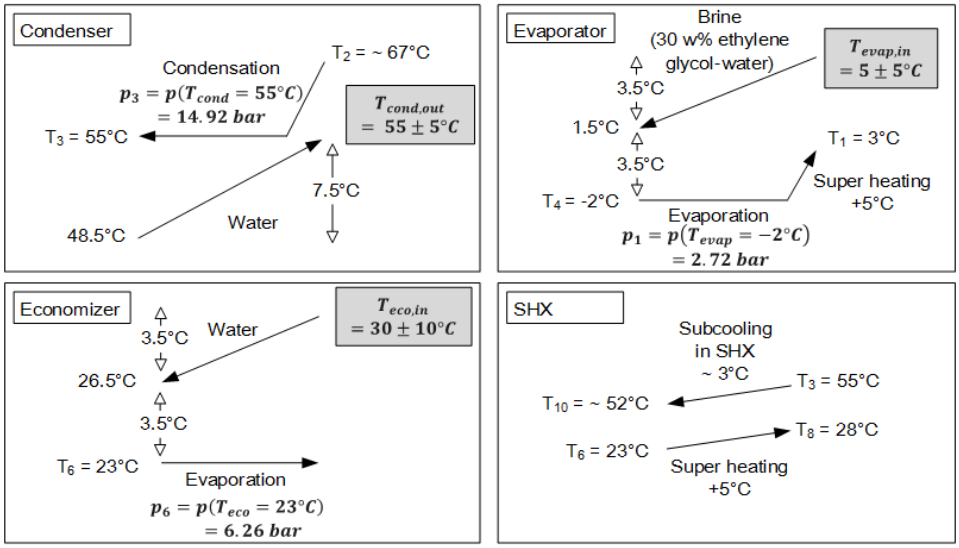

Figure 2: Temperature profiles in the heat exchangers at the design point with approach temperatures and temperature differences between water (brine) supply and return used in the simulation model

Table 4: Mass flow rates, UA-values, effectiveness, NTU, and heat capacities at design point conditions.

Parameter	Description	Unit	Cond	Eco	Evap	SHX
$\dot{m}$	water (brine) mass flow rates	kg/s	0.207	0.089	0.289	-
UA	heat transfer coefficient	kW/K	1.855	0.258	0.739	0.0073
ε	effectiveness	-	0.882	0.5	0.5	0.155
NTU	number of transfer units	-	2.14	0.69	0.69	0.18
$\dot{Q}$	heat capacity	kW	6.5	1.3	3.7	0.2

2.3 Compressor model

Non-dimensional numbers (Dixon and Hall, 2014) are used to plot the compressor maps, as the compressor characteristics depend on inlet pressure, inlet temperature, and the physical properties of the refrigerant (Table 5). The data used are based on predicted compressor maps data obtained by Javed *et al.* (2016). The following polynomial fit approximations, derived from linear regression calculations, have been used to fit the map data in the simulation model. The corresponding coefficients $A_{0\ldots5}$ and $B_{0\ldots8}$ of the polynoms are listed in Table 6. The R-squared values achieved are $R^2 > 99\%$.

$$\Pi_{low} = A_0 N_{low} + A_1 N_{low}^2 + A_2 \dot{M}_{low} N_{low} + A_3 \dot{M}_{low}^2 N_{low} + A_4 \dot{M}_{low} N_{low}^2 + A_5 N_{low}^3$$
$$\eta_{low} = B_0 + B_1 \dot{M}_{low} + B_2 N_{low} + B_3 \dot{M}_{low}^2 + B_4 N_{low}^2 + B_5 \dot{M}_{low} N_{low} + B_6 \dot{M}_{low}^2 N_{low} + B_7 \dot{M}_{low} N_{nd}^2 + B_8 N_{low}^3$$
$$\Pi_{high} = C_0 N_{high} + C_1 N_{high}^2 + C_2 \dot{M}_{high} N_{high} + C_3 \dot{M}_{high}^2 N_{high} + C_4 \dot{M}_{high} N_{high}^2 + C_5 N_{high}^3$$
$$\eta_{high} = D_0 + D_1 \dot{M}_{high} + D_2 N_{high} + D_3 \dot{M}_{high}^2 + D_4 N_{high}^2 + D_5 \dot{M}_{high} N_{high} + D_6 \dot{M}_{high}^2 N_{high} + D_7 \dot{M}_{high} N_{high}^2 + D_8 N_{high}^3$$

Table 5: Non-dimensional numbers used to plot the compressor maps ($\dot{m}$ = mass flow rate [kg/s], $\dot{M}$ = non-dimensional mass flow rate [-], n = rotational speed [rpm], N = non-dimensional rotational speed [-], Π = pressure ratio [-], η = isentropic efficiency [-], ρ = density at compressor inlet [kg/m^3], a = speed of sound at compressor inlet [m/s], D = tip diameter of the impeller [m], p_1, p_6, p_2 = pressures at compressor inlet and outlet [Pa]).

Non-dimensional number	1st stage compressor (*low*)	2nd stage compressor (*high*)
Non-dimensional mass flow rate	$\dot{M}_{low} = \dot{m}_{low}/\rho_{low} a_{low} D_{low}^2$	$\dot{M}_{high} = \dot{m}_{high}/\rho_{high} a_{high} D_{high}^2$
Non-dimensional rotational speed	$N_{low} = n_{low} D_{low}/a_{low}$	$N_{high} = n_{high} D_{high}/a_{high}$
Pressure ratio	$\Pi_{low} = p_6/p_1$	$\Pi_{high} = p_2/p_6$
Isentropic compressor efficiency	$\eta_{low} = (h_{2s} - h_8)/(h_2 - h_8)$	η_{high}=$(h_{9s} - h_1)/(h_9 - h_1)$

Table 6: Polynomial fit coefficients of the 1st (low) and 2nd (high) stage compressor maps (R^2 > 99%)

	Π_{low}	η_{low}	Π_{high}	η_{high}
Indices	**A**	**B**	**C**	**D**
0	9.714	0.6447	9.997	0.6846
1	-27.41	-11.42	-29.56	-9.572
2	-13.26	1.851	-13.78	1.388
3	-1126	-852.2	-1359	-996.6
4	199.8	-16.25	221.4	-14.17
5	41.81	239.3	44.91	242.7
6		1614		1879
7		-406.4		-415.3
8		23.87		21.05
R^2	**0.99994**	**0.99635**	**0.99995**	**0.99779**

3. SIMULATION RESULTS

3.1 COP calculation

The performance of the system is evaluated by calculating the heating COP of the circuit, which is defined as $COP = \dot{Q}_{cond}/W_{el,tot}$, whereas the total power $W_{el,tot}$ consumed by the turbocompressors is

$$W_{el,tot} = W_{el,low} + W_{el,high} = \dot{m}_{low}(h_9 - h_1) + \dot{m}_{high}(h_2 - h_8) \quad (21)$$

The graphs in Figure 3 show the influences of the different process parameters on the COP. As can be seen, the COP increases with higher source temperatures ($T_{evap,in}$ and $T_{eco,in}$), higher second heat source capacity (β), lower sink temperature ($T_{cond,out}$) and heating capacity $\dot{Q}_{cond}$. At the design point a COP of 4.3 is reached. Figure 3 also presents the relative COP increase as a function of β compared to a system without second source heat (COP_0 at $\beta = 0$). Overall, the addition of second source heat results in significant improvements on the COP. At the design point, a COP increase of 19% is achieved. A COP increase of up to 36% is reached under optimized temperature conditions.

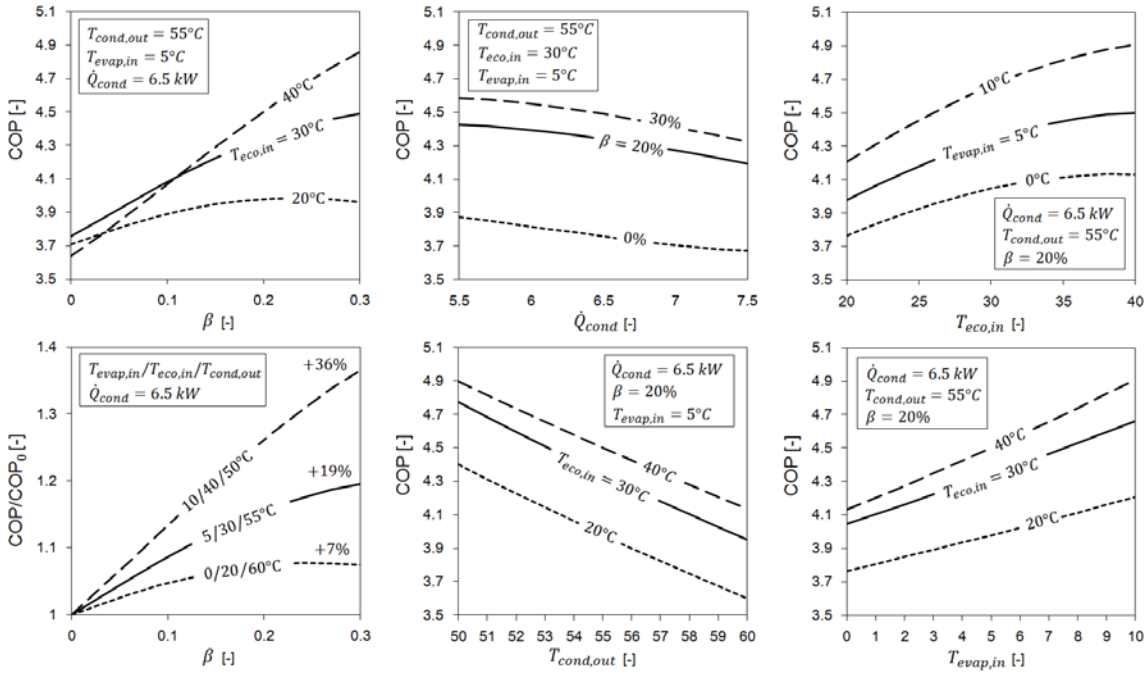

Figure 3: Influence of the process parameters $T_{evap,in}, T_{eco,in}, T_{cond,out}, \beta$ and $\dot{Q}_{cond}$ on the heating COP. COP/COP_0 indicates the relative COP increase compared to a system without 2nd source heat source ($\beta = 0$).

3.2 Heat pump operating range

Figure 4 presents the data of the predicted and fitted non-dimensional compressor maps for the first and second stage turbocompressors. The maximal achievable pressure ratios are about 3.5 for both compressors, which are limited by the maximum rotational speeds and the impeller sizes. The non-dimensional rotational speeds range from 0.27 up to 0.46 corresponding to about 160,000 to 270,000 rpm, respectively. As a reference, the black circles in each map indicate the conditions at the design point of the heat pump. The grey dots reveal the area of isentropic efficiencies > 76%. The predicted surge and choke margins are also depicted in the maps.

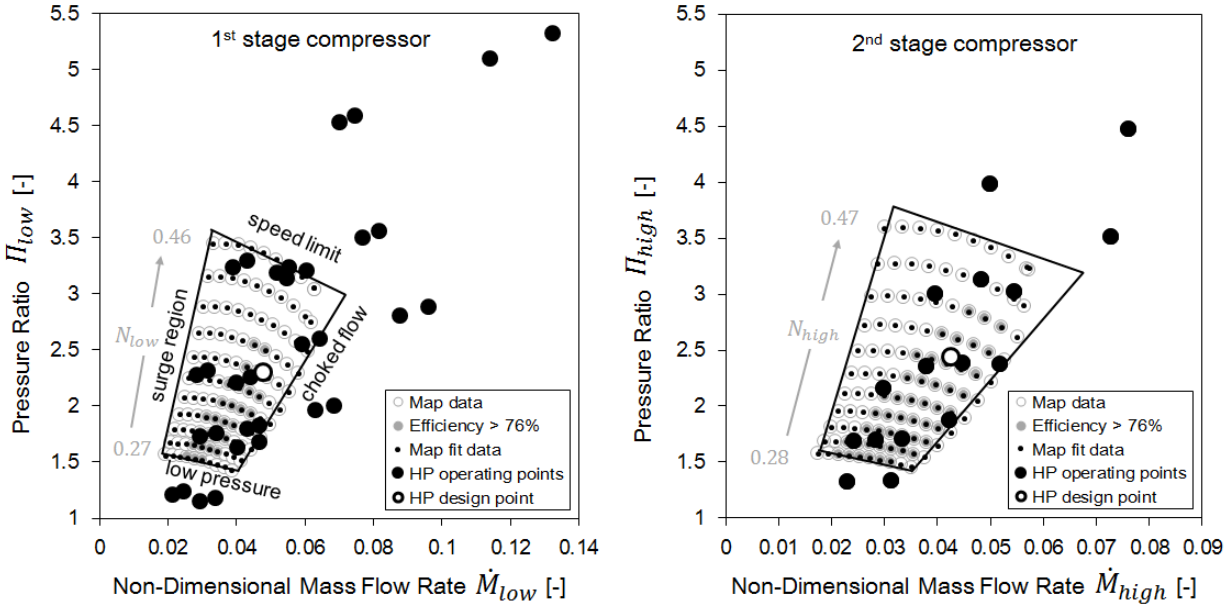

Figure 4: Predicted and fitted compressor maps for the first and second stage turbocompressors. Overlaid are the design point of the heat pump and the simulated operating points from the 2^5 factorial design of experiments.

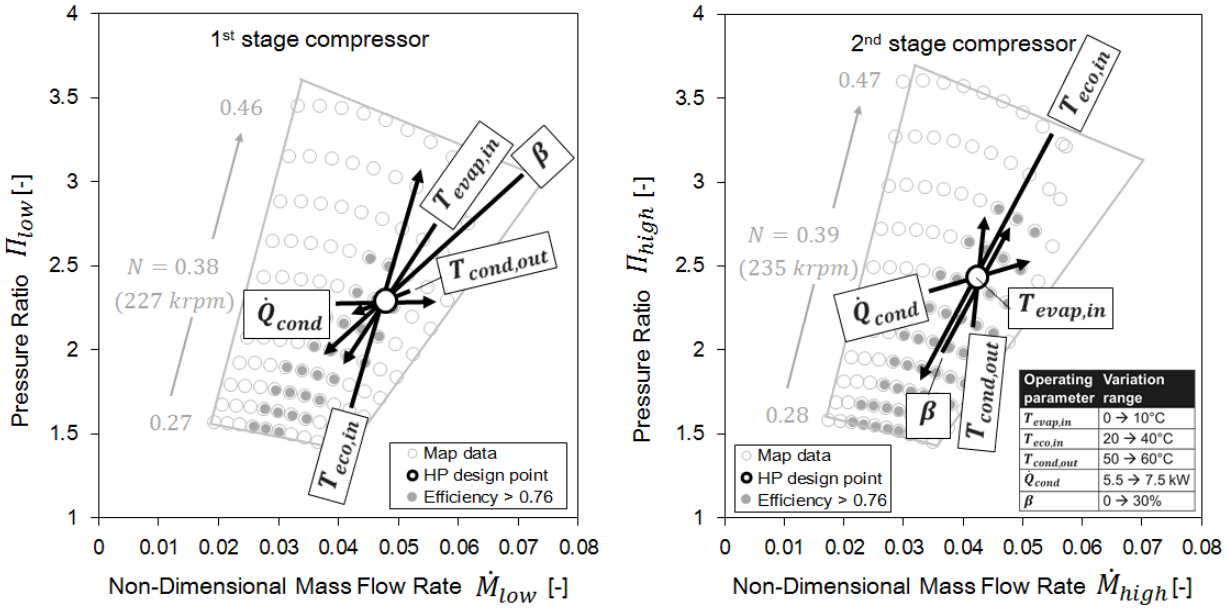

Figure 5: Compressor maps showing the influence of the parameter variations from the design point of the heat pump (black circle). The arrows indicate the variation ranges (shown in the table).

By varying of the 5 process parameters in their (±) variation ranges from the design point (according to Table 1), the operating range of the cycle was evaluated. This results in a 2^5 factorial experimental design (see Klein, 2011), which was used to generate a simulated cloud of operation points, plotted as black dots in the compressor maps (Figure 4).

As can be seen, most of the operating points fit the maps; however, some are out of the maps, especially those with high spreads between evaporation and condensation temperatures (T_{cond}, T_{int}, T_{evap}). Under these conditions, the resulting pressure ratios exceed the speed limits of the compressors. It is also noted that the operating points in the first stage are slightly shifted to the right of the map, e.g. towards larger mass flow rates. Some points even cross the choke margin. There, the compressor will not deliver the required power as the mass flow is choked.
As recognized by Schiffmann (2008), the application of a turbocompressor for driving a domestic heat pump is challenging, and clearly demands a wide range of pressure ratios and mass flows. A further optimization step would be required to narrow down the operating range of the heat pump to fit completely into the compressor maps.
Figure 5 shows the results of the parameter study based on the design point. In this sensitivity analysis, each input parameter was varied in its operating range while keeping the others constant. The arrows illustrate the results with increasing parameter value. The parameter variations move the operating point towards the following directions:

- $\dot{Q}_{cond}$ (5.5 kW → 7.5 kW) to higher mass flow rates in both stages,
- $T_{cond,out}$ ($50°C \rightarrow 60°C$) to higher pressure ratios in the 2nd stage,
- $T_{eco,in}$ ($0°C \rightarrow 10°C$) to higher pressure ratios in the 1st stage and to lower pressure ratios in the 2nd stage,
- $T_{evap,\text{in}}$ ($0°C \rightarrow 10°C$) to lower pressure ratios in the 1st stage, and
- β ($0\% \rightarrow 30\%$) to lower mass flow rates and pressure ratios in the 1st stage and to higher pressure ratios in the 2nd stage.

4. DESIGN CONSIDERATIONS

The simulation results are helpful to find appropriate control strategies to set up an experimental testing prototype as a continuation of this project. The two expansion valves EXV 1 and EXV 2 are important heat pump control devices to regulate superheating at the evaporator and the SHX outlets, i.e. at the compressor inlets. Depending on the operating conditions, the mass flow rates and pressure ratios need to be adjusted in the turbocompressors. Therefore, speed regulation by variable-speed motors has to be implemented to balance the variations in the process parameters. Speed control modulates mass flow capacity and achievable pressure ratios.
In addition, automatic compressor bypass systems need to be installed to further control the pressure ratios when heat from the second source is entering the heat pump system. Starting up a radial turbocompressor with an already existing pressure ratio (i.e. preset in the heat exchangers) may result in surge, with the refrigerant alternately flowing backward and forward through the compressor, accompanied by increased noise and vibration (ASHRAE, 2012). Prolonged operation under these conditions could damage the compressors (Carré, 2015). In order to avoid this situation, the compressors need to be started within the automatic bypass circuit, which prevents unstable surging and provides flow characteristics compliant with the compressor maps derived from Javed *et al.* (2016).

5. CONCLUSIONS

A system model was developed and programmed in EES software in order to evaluate the performance of a novel two-stage heat pump cycle with two miniature turbocompressors and an open economizer. The compressors were modeled as polynomial fit approximations based on predicted non-dimensional compressor map data. The heat exchangers were simulated using overall effectiveness-NTU models. The influence of the different process parameters on the COP and operating conditions was studied based on a 2^5 experimental design approach.
The simulation results reveal that the COP increases with higher source temperatures, higher second heat source capacity, lower sink temperature and heating capacity. At the design point, a COP of 4.3 is achieved. The addition of 30% of second source heat results in a 19% improvement on the COP compared to a system without second source heat. A COP improvement of up to 36% is achieved under optimized temperature conditions.
The second source heat and the heat sink capacity determine the required mass flow rates of the refrigerant from the compressors. The selected operating conditions, particularly the temperature levels of the evaporators and condenser, define the necessary pressure ratios of the compressors. Most operating points of the heat pump fit the compressor maps. Those with high spreads between evaporation and condensation temperatures result in pressure ratios that exceed the speed limits of the compressors. Narrowing down the operating range is required to fit the compressor maps completely. The availability of small-scale turbocompressors is foreseen paving the way to performance improvements in the field of domestic heat pumps by allowing the use of oil-free technologies in heat pump circuits and achieving high compressor efficiencies. In future work, the simulation model will be used to size the system components and set up an experimental testing prototype.

NOMENCLATURE

a	speed of sound	(m/s)
C	heat capacity	(kJ/kg K)
COP	coefficient of performance	(–)
D	tip diameter of the impeller	(m)
h	specific enthalpy	(kJ/kg)
rpm	rotational speed per minute	(1/s)
$\dot{M}$	non-dimensional mass flow rate	(–)
$\dot{m}$	mass flow	(kg/s)
n	rotational speed	(rpm)
NTU	number of transfer units	(–)
N	non-dimensional rotational speed	(–)
p	pressure	(kPa)
$\dot{Q}$	heat capacity	(kW)
T	temperature	(°C)
ΔT	temperature difference	(°C)
UA	UA-value	(kW/K)
W	electrical power of compressor	(kW)
x	quality	(–)
β	second heat source factor	(–)
ε	effectiveness	(–)
ρ	density	(kg/m^3)
Π	pressure ratio	(–)
η	isentropic efficiency	(–)

Subscripts

cond	condenser
eco	economizer
el	electrical
evap	evaporator
low	low stage, first (1st) stage
high	high stage, second (2nd) stage
in	inlet
out	outlet
SHX	suction line heat exchanger
sub	subcooling
sup	superheating
tot	total
1 … 10	thermodynamic states

REFERENCES

Arpagaus, C., Bless, F., Schiffmann, J., & Bertsch, S. S. (2016a). Multi-Temperature Heat Pumps – A Literature Review, accepted for publication on May 24, 2016. *International Journal of Refrigeration*. doi:10.1016/j.ijrefrig.2016.05.014

Arpagaus, C., Bless, F., Schiffmann, J., & Bertsch, S. S. (2016b). Multi-Temperature Heat Pumps – A Literature Review, Paper ID 2021. *International Refrigeration and Air Conditioning Conference, Purdue, R-04: Heat Pump Design and Assessment*.

ASHRAE. (2012). Chapter 38: Compressors. In *Handbook - HVAC Systems and Equipment* (pp. 1–38).

Bertsch, S. S., & Groll, E. A. (2006). Air Source Heat Pump for Northern Climates Part I: Simulation of Different Heat Pump Cycles, Paper 783. *International Refrigeration and Air Conditioning Conference*, 1–9. Retrieved from http://docs.lib.purdue.edu/iracc/783

Bertsch, S. S., & Groll, E. A. (2008). Two-stage air-source heat pump for residential heating and cooling applications in northern U.S. climates. *International Journal of Refrigeration*, *31*(7), 1282–1292. doi:10.1016/j.ijrefrig.2008.01.006

Carré, J.-B. (2015). *Experimental investigation of electrical domestic heat pumps equipped with a twin-stage oil-free radial compressor, Thèse N° 6764, École Polytechnique Fédérale de Lausanne, Switzerland*.

Danfoss Turbocor Compressors. (2013). *TURBOCOR centrifugal compressors for air-conditioning systems, www.turbocor.com, Datasheet S-BR-001-EN Rev. A (2-13)*.

Dixon, S. L., & Hall, C. A. (2014). *Fluid Mechanics and Thermodynamics of Turbomachinery, 7th edition*. Oxford, UK: Elsevier Inc.

Favrat, D., Nidegger, E., Reymond, D., & Courtin, G. (1997). Comparison single-stage and two-stage air to water domestic heat pump.pdf. In *IIF-IIR-Commission E2, with E1 & B2, Linz, Austria, 1997/4*.

GEA Process Engineering Inc. (2014). Evaporation Technology using Mechanical Vapour Recompression, brochure P02E 052003 04000.

Granwehr, E. V., & Bertsch, S. (2012). Heat pump. Patent WO 2012/040864 A1.

IEA. (2012). Industrial heat pumps, IEA Heat Pump Centre Newsletter, *Volume 30*, No. 1/2012, p. 15. Retrieved from www.heatpumpcentre.org

Javed, A., Schiffmann, J., Arpagaus, C., & Bertsch, S. (2016). Design of Oil-Free Turbocompressors for a Two-Stage Industrial Heat Pump under Variable Operating Conditions, Paper ID 1088. In *International Compressor Engineering Conference, Purdue, C-18: Centrifigal Compressors*.

Klein, B. (2011). *Versuchsplanung - DoE*. *Journal of Chemical Information and Modeling* (Vol. 53). Oldenbourg Verlag München. doi:10.1017/CBO9781107415324.004

Klein, S. A. (2012). Engineering Equation Solver, Academic Professional V9.206, F-Chart Software.

Klein, S. A., & Nellis, G. (2012). *Heat Transfer*. New York: Cambridge University Press.

Schiffmann, J. (2008). *Integrated Design, Optimization and Experimental Investigation of a Direct Driven Turbocompressor for Domestic Heat Pumps*. Thèse N° 4126, École Polytechnique Fédérale de Lausanne, Switzerland.

Schiffmann, J. (2014). Small-Scale and Oil-Free Turbocompressor for Refrigeration Applications. *International Compressor Engineering Conference, Paper 2354*. doi:http://docs.lib.purdue.edu/icec/2354

Schiffmann, J. (2015). Integrated Design and Multi-objective Optimization of a Single Stage Heat-Pump Turbocompressor. *Journal of Turbomachinery*, *137*(7), 071002. doi:10.1115/1.4029123

Schiffmann, J., & Favrat, D. (2006). High-Speed Low Power Radial Turbocompressor for Oil-Free Heat Pumps, Paper 1828. *International Compressor Engineering Conference*. Retrieved from http://docs.lib.purdue.edu/icec/1828

Schiffmann, J., & Favrat, D. (2009). Experimental investigation of a direct driven radial compressor for domestic heat pumps. *International Journal of Refrigeration*, *32*(8), 1918–1928. doi:10.1016/j.ijrefrig.2009.07.006

Schiffmann, J., & Favrat, D. (2010). Design, experimental investigation and multi-objective optimization of a small-scale radial compressor for heat pump applications. *Energy*, *35*(1), 436–450. doi:10.1016/j.energy.2009.10.010

Uhlmann, M., Heldstab, A., & Bertsch, S. (2014). OptiRef: Heat Pump with Two Heat Sources at Different Temperature Levels, Paper 2142. In *International Refrigeration and Air Conditioning Conference* (pp. 1–10).

Zehnder, M. (2004). *Efficient Air-Water Heat Pumps for High Temperature Lift Residential Heating, including oil migration aspects*. Thèse N° 2998, École Polytechnique Fédérale de Lausanne, Switzerland.

ACKNOWLEDGMENT

The authors thank the Swiss Competence Center for Energy Research on Efficiency of Industrial Processes (SCCER EIP) for their financial support.